Summer Programs Symposium

August 1st – August 2nd, 2018

Summer Program for Undergraduate Research (SPUR)

Julia Williams – University of Wisconsin – Parkside
Jieqing Zhu, PhD
Department of Biochemistry

Ligand induced β3 integrin headpiece opening in solution

Background and Aim

Integrins are cell surface receptors that are essential for connecting cells with the extracellular matrix or neighboring cells. Integrin is composed of two subunits, an α and a β, each containing headpiece, leg piece, transmembrane, and cytoplasmic domains. In the resting state, integrin adopts a bent conformation with closed headpiece. Upon activation, integrin undergoes two major conformational changes, headpiece extension and headpiece opening, which are essential for integrin to mediate cell adhesion, spreading, and migration. Integrin conformational changes are a dynamic reversible process, which is essential for integrin activation and deactivation. However, how ligand binding and disassociation affect the reversible integrin conformational changes remains poorly defined. In this study, we used two model integrins, platelet αIIbβ3 and endothelial αVβ3, to examine how ligand binding and disassociation affect the headpiece opening and closing in solution. αIIbβ3 and αVβ3 integrins, through recognizing a RGD or RGD-like motif in their ligands, play important roles in platelet aggregation, and growth and survival of endothelial cells. A synthetic GRGDSP peptide, derived from the β3 integrin ligand fibronectin, was used as ligand for both αIIbβ3 and αVβ3 integrin.

Methods

Both αIIbβ3 and αVβ3 headpiece constructs contain the β-propeller and thigh domains of α subunit, and the βI, PSI, hybrid, and I-EGF1 domains of β subunit, with a C-terminal coiled-coil tag and a Strep-Tactin affinity tag (for αVβ3), and 6XHis tag (for both αIIbβ3 and αVβ3). The headpiece constructs were stably expressed as secreted proteins in CHO Lec cells. The αVβ3 headpiece protein was purified from the cell culture supernatant by Strep-Tactin column. The αIIbβ3 headpiece protein was purified by antibody-agarose column or Ni-NTA column. The tags were then removed by digestion using Tobacco Etch Virus (TEV) protease (for αVβ3) or chymotrypsin (for αIIbβ3). The untagged headpiece proteins were finally purified by size exclusion chromatography. The purified headpiece proteins at 1 μM were measured by dynamic light scattering (DLS) in the absence or presence of different concentrations of GRGDSP peptides. DLS measures the hydrodynamic radius (or Stokes radius) of protein in solution, which correlates with the large-scale conformational change.

Results

In the presence of GRGDSP, both the αIIbβ3 and αVβ3 headpiece changed from a closed to an open conformation, indicated by the increase of hydrodynamic radii measured by DLS. A high affinity αIIbβ3-specific RGD-mimetic drug, namely GR14, which does not induce integrin conformational changes, was used as a competitor to disassociate GRGDSP from the integrin headpiece. Our data demonstrate that the revisable close-to-open transition of integrin headpiece can be measured by DLS in solution, which provides a suitable approach to analyze the dynamic conformational changes of integrin using purified proteins.

Chandler McElrath – Carroll University
William Campbell, PhD
MCW Department of Pharmacology and Toxicology

Characterization of G-Protein Coupled Receptors for EET Isomers

Epoxyeicosatrienoic acids (EETs) are cytochrome P450 metabolites of arachidonic acid. These lipid-based compounds act as important signaling molecules that are released from vascular endothelial cells (ECs), and act on specific endothelial and smooth muscle receptors. On smooth muscle cells, EETs induce membrane hyperpolarization, prevent calcium influx and cause vasorelaxation. Therefore, blood vessels dilate, and blood pressure is lowered. The EET receptor(s) is indicative of a G-protein coupled receptor (GPCR). However, this EET receptor(s) has yet to be identified. Previous data indicate that 14,15 EET binds a 47 kD protein in U937 cells. We hypothesize that photoaffinity labeling can be used to identify EET binding proteins, and that 11,12-EET and 14,15-EET may bind their own unique receptors.

Photoaffinity labeling and click chemistry were used to investigate EET binding in human cells. Five photoaffinity probes containing the basic 14,15- or 11,12-EET agonist structures with an additional photoactive group (benzophenone or diaziridine) and a click moiety (azide) were studied. Following photoprobe binding with its receptor, exposure to UV light resulted in a covalent crosslink of the photoprobe to the receptor protein(s). A biotin group was then linked to the probe's click moiety via a copper catalyzed reaction. Protein samples were resolved by SDS-PAGE, streptavidin HRP bound to biotin, and proteins visualized by chemiluminescence.

A number of protein bands over a range of molecular weights were detected by this method in U937 cells, human ECs, and HEK293 cells. To distinguish proteins that specifically or non-specifically bind the EET photoprobes, samples were treated with photoprobes with and without excess 11,12- or 14,15-EET to complete for binding or were not exposed to UV light to prevent photocrosslinking. Co-incubation with EETs or no UV light reduced labeling by the photoprobe to proteins that specifically bind the EETs but did not affect non-specific binding. When U937 cell membranes incubated with the 14,15-EET photoprobes, specific binding was detected to 90, 55, and 47 kDa proteins. In contrast, no specifically bound proteins were detected in these cell membranes with the 11,12-EET photoprobes. Under these same conditions however, protein bands were visualized in human ECs near 60 kD and HEK293T cells near 150, 60, and 50 kDa. Visualization of these protein bands differed when crosslinking was performed with cell membranes versus whole cells. Receptors of these molecular weights may prove to be interesting targets for future studies. HEK293 cells are commonly used to overexpress proteins of interest in receptor identification, but this cell type may not be ideal for studying EET receptors if the receptor is indigenously expressed. These studies indicate that 11,12- and 14,15-EET photoprobes bind different proteins in some cells and may therefore have different receptors.

Future studies will concentrate, purify and identify the specific proteins that bind 11,12- or 14,15-EET from U937 cells and ECs. Expanding research in this area will lead to a better understanding of the pathways activated by the EETs, the physiological impact of EETs and lead to the development of new therapeutic agents.

Dustin Cloutier – Carroll University
Julian Lombard, PhD
MCW Department of Physiology

Characterization of Mas1 Receptor Knockout Rat: A Novel Model to Study Hypertension

The renin-angiotensin system (RAS) regulates blood pressure (BP) via multiple hormones and receptors, including the hormones angiotensin II (ANGII) and ANG-(1-7) as well as the receptors AT1R and Mas1R. High levels of ANGII are associated with endothelial dysfunction, hypertension, cardiovascular disease, and related harmful effects. On the other hand, recent studies have shown that chronically low levels of ANGII also cause endothelial dysfunction. Due to a compromised RAS, salt-sensitive (SS) individuals (animals and humans) often experience chronically low ANGII levels even on a low salt (LS) diet. However, restoring normal plasma ANGII levels via chronic ANGII infusion restores endothelial function in SS rats and normotensive rats with high salt (HS)-induced ANGII suppression. ANG-(1-7) also restores normal endothelial function via the Mas1R. Several knockout (KO) strains of rats have been generated as experimental models for studying the RAS. To assemble a complete arsenal of strains, adding a Mas1R KO is crucial. A Mas1R KO rat on a SS genetic background was recently generated by inducing a frameshift mutation in the Mas1R gene. This novel strain will provide a powerful tool to understand the role of chronically low plasma ANG-(1-7) levels in the development of endothelial dysfunction and hypertension in SS individuals. Our goal was to phenotype the Mas1R KO rat and investigate the role of ANG-(1-7) binding to the Mas1R in regulating endothelial function. We hypothesized that ANG-(1-7) would improve endothelial function in wild type (WT) rats but not in KO rats lacking the Mas1R. Mas1R WT rats should also exhibit reduced endothelium-dependent dilation vs. normotensive Sprague-Dawley (SD) rats due to reduced RAS activity leading to suppressed ANG-(1-7) (and ANGII) levels, thereby limiting Mas1R activation.

Mas1R KO and WT rats were maintained on low salt (0.4% NaCl) diets to evaluate endothelial dysfunction without an elevated BP in the SS genetic background. Middle cerebral arteries (MCA) were isolated to assess endothelial function *ex vivo* using the endothelium-dependent vasodilator acetylcholine (ACh). Appropriate vasodilation was considered an indicator of proper endothelial function.

Western blots were performed to evaluate Mas1R expression in Mas1R WT and KO rats. Both exhibited similar banding patterns which supports that the functional KO was generated via a frameshift mutation which did not drastically alter molecular weight, but still rendered the Mas1R non-functional. The Mas1R WT exhibited significantly greater dose-dependent vasodilation compared to their KO counterparts ($p<0.05$), but this was still significantly less than the maximum dilation seen in normotensive SD control rats ($p<0.05$).

These findings both help to better understand the Mas1 KO to establish it as a viable model for future studies and support that the Mas1R plays a protective role in the endothelium, Mas1R activation promotes endothelial function, and Mas1R agonists are a promising treatment for hypertension.

Keywords: Renin-angiotensin system, angiotensin II, angiotensin (1-7), endothelial function, vasodilation, salt-sensitivity

Christina M. Mecca[1], Mohamad Kahil[2], and Bonnie Dittel[2,3].

[1]Department of Biology, Neuroscience Program, The University of Scranton;
[2]Department of Cellular and Molecular Immunology,
[3]Department of Microbiology and Immunology, Medical College of Wisconsin

---

Can Chronic Lymphocytic Leukemia (CLL) Exhibit Regulatory B Cell Function?

Abstract: Leukemia is a cancer type that originates in bone marrow, where blood cells are produced. B cells are immune cells that are derived from the bone marrow, and typically protect the body from potential harmful pathogens/antigens. However, B cells can also regulate immune responses negatively. B regulatory cells, or Breg, are later matured B cells. One type of Leukemia is B cell Chronic Lymphocytic Leukemia (CLL). CLL is the most common leukemic cancer in adults in North American and Europe. CLL most commonly manifests in the elderly population, producing obstacles in treating this disease. To effectively treat this disease, less harsh, and more tolerable therapies are needed. CLL cells are characterized by the production of $CD5^+$ $CD23^+$ IgM^+ IgD^+ B lymphocytes. There are many characteristic features of CLL. Firstly, there is a significant increase in regulatory T cells (Treg) in the blood of CLL patients, but the mechanism of this increase is still unknown. This increase in the Tregs may prevent immune system detection and clearance. Moreover, the tumor necrosis factor ligand superfamily member 18 (TNFSF18) or GITRL is highly expressed in CLL among other leukemic cells. Recently, the Dittel lab discovered a new mouse splenic B cell subpopulation that can maintain Treg hemostasis and resolve the symptoms of EAE autoimmune disease. This subpopulation is characterized by low IgD expression and high expression of GITRL (BD_L.). BD_L may have a similar phenotype to these CLL cells. Based on B cell studies in both rodent and human models, it is hypothesized that $IgD^{low/-}$ $GITRL^{hi}CCR7^+$ CLL will exhibit Breg activity and induce proliferation of Treg thereby hampering their clearance by the immune system. The first step in exploring this hypothesis was to first screen human CLL lines for CCR7, GITRL, IgM, and IgD. Through RT-PCR and Flow Cytometry. It was found that the CLL human cell lines: WA-OSEL and CI both expressed low levels of IgD and IgM, and high levels of GITRL and CCR7, suggesting that these cell lines are phenotypically similar to BD_L. Furthermore, the high expression of GITRL and CCR7 may be utilized to enhance the expansion and proliferation and expansion of Tregs in CLL. Understanding CLL's mechanism may aid in the development of new anti-tumor agents by inhibiting and interfering Treg expansion, without causing autoimmunity.

Keywords: CLL, Breg, Treg, GITRL, CCR7, IgD, IgM

Nnenna S. Nwaelugo – Northwestern College
Brian Smith, Ph.D.
MCW Department of Biochemistry

Expression and Purification of nNOS and nNOS Derivatives

Nitric-oxide synthases (NOS) are a family of enzymes responsible for producing nitric oxide, an important regulator and mediator of numerous processes in the nervous, immune, digestive, and cardiovascular systems. There are three mammalian NOS isoforms, inducible NOS (iNOS), endothelial NOS (eNOS), and neuronal NOS (nNOS), that regulate immune and inflammatory responses, blood circulation and neuronal activity respectively. NOS activation requires the calcium-dependent signalling protein calmodulin (CaM), and we hypothesize that NOS function is regulated through a series of conformational equilibria. While several previous studies have identified multiple conformations of NOS, the sequence of conformational states and timing of interconversion between states is unknown, and it is still unclear how each conformational change correlates with the enzyme's catalytic cycle. The aim of this project is to directly track the conformational dynamics of nNOS in order to understand the sequence and kinetics of interchange, how conformational dynamics regulate NOS activity, and whether the variance of conformational dynamics can explain the differences in activity between NOS isoforms.

To enable single-molecule spectroscopic studies of nNOS conformational states, several recombinant *E. coli* expression constructs were generated. Wild type, AVI-tagged, and R1229E nNOS were recombinantly expressed in *E. coli* and purified using calmodulin sepharose affinity and size-exclusion chromatography. nNOS activity was assayed by spectrophotometrically monitoring the NO-dependent conversion of oxyhaemoglobin to methaemoglobin. Activity assays demonstrated that the addition of an AVI-tag, which will allow attachment of nNOS to avidin-coated slides for single-molecule fluorescence analysis of conformational dynamics, does not impair nNOS activity. Conversely, the R1229E mutant was found to be inactive, which is consistent with the charge-reversal mutation inhibiting FAD to FMN electron transfer. SDS-PAGE gels, western blots using an antibody specific for the *C*-terminal of nNOS, and *N*-terminal biotinylation experiments demonstrated a *C*-terminal truncation of approximately half of the purified nNOS protein. Size exclusion chromatography was consistent with the formation of mixed dimers through the oxygenase domains of the full-length and truncated forms of the proteins, which would complicate interpretation of experiments designed to probe the conformational dynamics of nNOS. Therefore, future experiments will be aimed at optimising expression and purification to eliminate or minimize this undesired truncation.

Chase Castro – University of Missouri
Rebekah Gundry, PhD
MCW Department of Biochemistry

Simplified protocol for standard peptide (SP2) cleanup: An optimized cleanup method using carboxylate coated paramagnetic beads

Background

Preparation of samples in the field of proteomics often utilizes reagents that impede the analysis of the samples by Liquid Chromatography – Mass Spectrometry (LC-MS). These substances include detergents and chaotropes, used in sample digestion and enrichment that can negatively affect performance of the instrument, as well as analysis of the sample. Other methods have been described such as protein precipitation, and reversed-phase liquid chromatography, however each method has inadequacies as protein precipitation produces protein pellets that are difficult to re-dissolve, while reversed-phase liquid chromatography can concentrate, instead of remove common detergents. Using carboxylate-modified paramagnetic particles, contaminants can be removed and peptide can be eluted into LC-MS friendly mobile phase. This study aimed to systematically evaluate experimental parameters of carboxylate-modified paramagnetic particles in order to optimize the workflow and develop a detailed protocol that can be implemented for reproducible results.

Method

Recovery of a tryptic digest sample cleaned by adsorption onto GE Healthcare Life Sciences Sera-Mag carboxylate modified paramagnetic beads was evaluated using a Pierce Quantitative Fluorometric Peptide Assay. More than 15 experimental variables were evaluated by performing titrations of bead and sample amounts to identify the relationship between particles:peptide ratio and recovery, as well as performing a range of modifications to particle type, binding temperature and starting concentration, wash volumes, elution volume and organic concentration, and time and mixing during elution and binding. Data were acquired on a Thermo Orbitrap Fusion Lumos and analyzed by ProteomeDiscoverer2.2.

Results

A logarithmic correlation between particles:peptide ratio and percent of sample recovery was observed. A ratio of 50:1 achieved ~80% sample recovery. Some improvements were made to the binding conditions by improving the mixing and elution. Washing volume did not negatively affect the percent recovery and modifications were made to the protocol with respect to recommendations for particle:peptide ratio and elution volume in order to increase percent recovery.

Conclusion

A partially optimized procedure was used on Tandem Mass Tag labeled samples contaminated with dominating polymers that were nearly undetectable after cleanup. The optimized protocol increased recovery to above 90%. SP2 represents a viable alternative to reversed-phase chromatography for routine preparation of peptide samples for mass spectrometry.

Corbin Schroeder – University of Wisconsin Platteville
Brian Volkman, PhD
MCW Department of Biochemistry

Computational design of protein therapeutics

Chemokines are small soluble proteins whose main function is in controlling cell migration, as well having benefits in pharmaceuticals. The chemokine CXCL12 aside its receptor CXCR4, is shown to play a major role in stem cell homing and breast cancer metastasis. The dimeric form of the chemokine has the opportunity to be beneficial as a therapeutic, as it has been shown to disrupt chemotaxis of cancerous cells. However, the dimeric form of the chemokine has trouble outcompeting the wild type chemokine to bind to CXCR4. The hypothesis is that the chemokine can be engineered to increase affinity with the N-terminus of the receptor. To determine whether this is true, we used a computational tool to test different mutations. The main computation tool used in running the experiments was a program called Rosetta. Rosetta allows different designs of the proteins to be made and different mutations can be tested. Computational runs can be made before using materials to recreate the proteins in a lab setting. Using a python script, the energy score, binding energy, and binding density for each mutation can be recorded. Box plots are then created as well as Per Energy Residue bar graphs. The results of the design runs showed that there were five possible mutations that would increase affinity to the chemokine receptor. Hotspots on the chemokine were spotted around the 60^{th}, 64^{th}, and 68^{th} residues of the dimer. The designs ranged from a Rosetta Energy Score of +6 to +1.5. The higher the energy score difference the better the fit that residue is in the chemokine. The binding energy and binding density for each design also increased by an average of 0.5 Rosetta score. Overall the results found show a possibility of increasing affinity to the dimeric form of the chemokine. Results would need to be run experimentally to gauge the effectiveness of the mutations in vitro. This can be crucial to finding a way to implement the dimeric form of the chemokine into pharmaceuticals at a reasonable concentration. The most important finding in this study is the opportunity Rosetta opens up for protein design and the possibility of saving money by running computational experiments before lab experiments. In conclusion, chemokines can be engineered to fit a certain need and benefit future pharmaceutical research.

John Happ – Whitman College
Jennifer S. Stancill, PhD
MCW Department of Biochemistry

Peroxiredoxin III and NADPH-generating Enzymes: Obligatory Components of the Peroxiredoxin/Thioredoxin Antioxidant System

Background

Insulin-producing beta cells are thought to be damaged by oxidative stress during the pathogenesis of both type 1 and type 2 diabetes mellitus. Reactive oxygen species (ROS), namely hydrogen peroxide (H_2O_2), are primary mediators of oxidative stress that are generated as by-products during mitochondrial electron transport. Contrary to long-standing dogma, our recent studies have shown that beta cells display a robust detoxification system in response to ROS. Our data suggest that pancreatic beta cells utilize the peroxiredoxin/thioredoxin antioxidant system, as inhibition or depletion of thioredoxin reductase or cytoplasmic peroxiredoxin 1 (*Prdx1*), sensitizes beta cells to continuously generated H_2O_2. Since mitochondria are a major source of H_2O_2 generation, we hypothesize that mitochondrial peroxiredoxin 3 (*Prdx3*) protects beta cells from oxidative damage. Additionally, because this system is dependent upon NADPH to reduce H_2O_2, we hypothesize that depletion of one or more of three major NADPH-generating enzymes, isocitrate dehydrogenase 1 (*Idh1*), malic enzyme 1 (*Me1*), and glucose-6-phosphate dehydrogenase (*G6pd*), will sensitize beta cells to H_2O_2-mediated damage.

Method

Specific siRNAs against rat *Prdx3, Idh1, ME1, or G6PD* were reverse transfected into INS 832/13 cells (a rat beta cell line) to knockdown the respective genes. H_2O_2 was delivered continuously using either glucose oxidase, to generate H_2O_2 in the media, or menadione, to generate H_2O_2 in the mitochondria. H_2O_2 concentration was measured using Amplex Red. Cell viability was measured via the neutral red dye uptake assay. Knockdown efficiencies were determined using quantitative real-time PCR.

Results

INS 832/13 cells become more sensitive to H_2O_2 generated by menadione when *Prdx3* is depleted, with 50% death occurring between 30-40 μM menadione. However, *Prdx1* depletion had a greater impact on cell viability, with 50% death occurring around 20 μM menadione. Combined knockdown of *Idh1, Me1,* and *G6pd* sensitized cells to continuously-generated H_2O_2 and correlated with elevated levels of H_2O_2 in the media.

Conclusion

These results support the hypothesis that *Prdx3* protects beta cells from H_2O_2 -mediated damage, but to a lesser extent than cytoplasmic peroxiredoxins, such as *Prdx1*. Given the role of low concentrations of H_2O_2 in promoting glucose stimulated insulin secretion, we speculate that beta cells express the mitochondrial *Prdx3* at lower levels than the cytosolic *Prdx1* to allow H_2O_2 to diffuse into the cytoplasm during oxidative phosphorylation, where it may play a signaling role. Furthermore, our results suggest that *Idh1, Me1, and G6pd,* which maintain a cellular store of NADPH, are obligatory components of the peroxiredoxin/thioredoxin antioxidant system within beta cells.

Austin Goff – Utah State University
Matt Scaglione, PhD
MCW Department of Biochemistry

Mitochondrial Ubiquitination by Ube2w and its Role in Neurodegeneration

Neurodegenerative diseases are debilitating disorders that alter basic neurological functions, such as cognition, movements, and memory. Protein misfolding, protein aggregation, and mitochondrial dysfunction are all hallmarks of many neurodegenerative diseases which include Alzheimer's Disease (AD), Parkinson's Disease (PD), Huntington's Disease (HD), and Amyotrophic Lateral Sclerosis (ALS). The ubiquitin-proteasome system (UPS) has been shown in these diseases to clear misfolded, damaged, or defective proteins by the addition of ubiquitin to the target protein, which acts as the signal for degradation by the proteasome. Ubiquitination occurs in a coordinated cascade of three proteins: ubiquitin-activating enzyme (E1), ubiquitin-conjugating enzyme (E2), and ubiquitin-ligase enzyme (E3). Among these, the E2 enzymes play a central role in where and how the attachment of ubiquitin (Ub) occurs on the target protein. Ube2w, a unique E2, has been the only identified E2 enzyme to ubiquitinate the N-terminus of substrates. More interestingly, Ube2w contains a specific mitochondrial localization motif. Classically, ubiquitination is known to occur within the cytosol and nucleus. However, it was recently shown that ubiquitination steps occur within the mitochondria. Since mitochondria health has been tied to neurodegenerative diseases, it is critical to understand the potential role the UPS plays in maintaining proteostasis. A green-fluorescent protein (GFP) tagged Ube2w was transfected into HEK293 cells and imaged using both fluorescent and confocal microscopy to assess co-localization of Ube2w and mitochondria. Upon fluorescent imaging, cells displayed multiple focal puncta, demonstrating possible localization within the cell. Western blotting was then used to determine the presence of any Ube2w cleavage, consistent with mitochondrial translocation. Different isoforms of Ube2w were used to determine any differences in translocation activity. Western blots demonstrated that cleavage occurs and differs between each Ube2w isoform. While it is apparent that the E2 enzyme Ube2w employs a specific and unique role in the ubiquitin-proteasome system, further investigation is required to fully understand the consequences of mitochondrial ubiquitination and its role in neurodegenerative diseases.

Jeannette Ingabire – Mount Mary University
Ranjan Dash, PhD
MCW Department of Biomedical Engineering

Computational Modeling of Cardiac L-Type Ca^{2+} Channel Function

Background: L-type Ca^{2+} channels (LCC) are primary pathways for Ca^{2+} influx into cardiac cells, and hence play an important role in cardiac (dys)function. Specifically, these channels are vital for modulation of action potentials and regulation of other cellular dynamical processes (e.g. excitation-contraction coupling). Pathophysiology associated with LCC include cardiac arrhythmia and Timothy Syndrome. In cardiac cells, Ca^{2+} influx is regulated by voltage (V-mode) as well as by Ca^{2+} (Ca^{2+}-mode). These regulation mechanisms are referred to as the calcium-dependent inactivation (CDI) and voltage-dependent inactivation (VDI). A quantitative understanding of these regulation mechanisms is critical for improving our understanding of cardiac physiology and pathophysiology associated with LCC (dys)function.

Methods: The purpose of this study was to quantitatively understand VDI and CDI mechanisms using a previously developed mathematical model (Markov model) which has four closed states (C0-C3), one open state (O), and two inactivation states (Ivs, Ivf) for VDI, along with a parallel Ca^{2+} mode for CDI. The VDI mode of this model was broken down into 3 reduced models: models 1, 2, and 3 to examine whether all LCC states and/or kinetic parameters are necessary to describe VDI. Ordinary differential equations (ODEs) for the models were derived using the law of mass action. MATLAB was used to solve the ODEs and scrutinize various ion currents via LCC and its transition states dynamics that govern VDI. Model simulations were made and compared to experimentally-observed kinetic and dynamic data on LCC function characterizing VDI. Further extension of the models was made to study CDI.

Results: Model simulation results showed that model 3 best fits the experimental data regarding VDI at all voltages. In terms of current dynamics, model 1 had the most ion current at low voltages (e.g. -30 mV). However, the difference in the current dynamics between the 3 models decreases as voltage increases (e.g. to 0 mV and +30 mV). At high voltages, LCC mostly transitions to the Ivs state, characterizing VDI. Inclusion of Ca^{2+} mode further inactivated LCC with Ca^{2+} as charge carrier, characterizing CDI.

Conclusion: Based on our model simulation results and the analyses, model 3 best represented the VDI of cardiac LCC. Therefore, all states (C0-C3) are important, consistent with LCC structure. The extended model with parallel Ca^{2+} mode also well described the CDI mechanisms. Further analysis is necessary to mathematically define LCC function which will have significant role in quantitatively understanding cardiac (dys)function.

Jessica DuVal – University of Wisconsin-Stout
John Henry Dasinger, PhD and David Mattson, PhD
MCW Department of Physiology

Dahl salt-sensitive rats maintained on a wheat gluten diet are protected from the development of maternal syndrome.

Preeclampsia (PE) is a pregnancy-specific disorder that is defined as developing hypertension and proteinuria after the 20th week of gestation. There is an increased risk prevalence of PE in women with preexisting kidney disease and hypertension. The way in which PE develops is unknown, but it is thought that it may be a two-step process in which the spiral arteries in the placenta are improperly remodeled, leading to the progression of maternal syndrome. A recently established model of PE is the Dahl Salt Sensitive (SS) rat, sustained on a 0.4% NaCl (low salt) casein-based diet. The Dahl SS rats exhibit a pregnancy-specific elevation in blood pressure and proteinuria compared to their virgin controls. Interestingly, our laboratory has previously shown that diet can impact the severity of salt sensitive hypertension and renal damage. When rats are bred and maintained on a purified AIN-76A wheat gluten (WG) diet, there is an attenuation in preeclamptic phenotypes (e.g. hypertension and renal damage) compared to rats maintained on the casein-based diet; moreover, we have previously demonstrated that adaptive immune mechanisms are important in the establishment of the maternal syndrome in the SS rat. Since rats fed the WG diet exhibited a protection from hypertension and renal disease which is dependent upon immune mechanisms, we tested the hypothesis that female rats fed the WG diet would have an attenuation of factors related to immune activation. Taking the diets of the rats into consideration, we wanted to investigate the presence of interleukin 1 beta (IL-1β), a proinflammatory cytokine, in the placenta of both SS and WG mothers. We hypothesized that the presence of IL-1β would be greater in the SS rats than in the WG rats. By isolating protein from SS and WG samples (n=3/group), identifying IL-1β via Western Blot analysis, and using beta-actin as a control to normalize the protein sample sizes, we found a 4.1-fold change in the presence of IL-1β in the placentas of SS rats on the casein diet compared to WG rats. Although further research is needed, this preliminary study indicated that inflammation levels were different in the two rat strains and could play a significant role in explaining why the WG rats are protected from PE.

Jourdan Valkner– Winona State University
Erica Woertz and Joseph Carroll, PhD
Advanced Ocular Imaging Program
MCW Department of Ophthalmology & Visual Sciences

Investigating Foveal Structure in Amblyopia

Background. Amblyopia is defined as a reduction in best-corrected visual acuity in one eye without apparent change in the ocular structures. It is most commonly caused by form deprivation in early childhood due to high refractive error, strabismus, or light deprivation. Although it is known that amblyopia is a neurological disorder, it is unclear whether amblyopia causes subtle structural changes in the eye. Here, we examined foveal structure in patients with amblyopia to see if any structural differences exist between amblyopic eyes and their fellow eyes.

Methods. Four subjects with unilateral amblyopia were recruited for this study. Refractive error was measured using a Topcon Autorefractor and subjective refraction, and axial length was measured using the Zeiss IOL Master. Cirrus HD-OCT scans were used to measure the depth, volume, width, slope, and area of the foveal pit. Adaptive optics scanning light ophthalmoscopy (AOSLO) was performed on three of the four subjects and used to measure peak cone density. Each subject's amblyopic eye was then compared to the fellow eye using a Wilcoxon matched pairs signed rank test.

Results. While axial length appeared to differ between amblyopic eyes and fellow eyes, this difference was not significant ($p = 0.125$). No significant differences were observed between the amblyopic eye and the fellow eye for foveal pit depth ($p = 0.625$), diameter ($p > 0.999$), slope ($p = 0.375$), volume ($p = 0.875$), or area ($p > 0.999$), nor was there a significant difference in peak cone density ($p = 0.250$).

Conclusion. No significant differences in foveal structure were found between amblyopic eyes and fellow eyes, thus this study does not provide evidence that amblyopia causes structural changes to the eye. However, this study was performed on a small sample size, so additional work is needed to study foveal structure in a larger cohort.

Michelle Lazar – University of Wisconsin Madison
Dr. Aron Geurts, PhD
Dr. Mike Flister, PhD
MCW Department of Physiology

The Clustered Regularly Interspaced Short Palindromic Repeats (CRISPR)-Cas9 system has recently been the forefront method for genomic editing. It allows for precise genomic editing and efficient creation of knock-out (KO) organisms. However, the CRISPR-Cas9 system has failed to produce high levels of efficiency for fragment knock-ins (KI). In order to increase the efficiency a Cas9-monomeric streptavidin fusion (cas9-mSA) was used. This cas9-mSA fusion was used along with a biotinylated repair template in the hopes of using the unusually strong bond between mSA and biotin to increase genetic editing efficiency. Rat embryonic stem cells (rESCs, SSGFP line 5-Passage 9) were thawed from cryopreserved stock, and cultured on mitomycin C-treated mouse embryonic fibroblasts (MEF) with 2i medium (N2B27 medium containing 1μM MEK inhibitor, 3μM GSK3 inhibitor, 10μM forskolin and 1,000 U/mL rat LIF supplement). Cells were passaged a minimum of 2 times before transfection. Rat ESCs were harvested after trypsinization/centrifugation, and approximately $5x10^5$ cells were resuspended with 300ul of transfection medium. Transfection complexes were comprised of 3μg cas9- mRNA or protein and 3ug sgRNA in 150 μL of FBS-Free medium (1:1 mixture of DMEM/F12 and Neurobasal® medium) and 6μL Lipofectamin® in 150uL of FBS-free medium. The goal of this experiment is to convert 2 amino acids to allow for the conversion of green fluorescent protein (GFP) to blue fluorescent protein (BFP) The groups for transfection were as follows: 1) Cas9 ribonucleorprotein (RNP) with single-stranded oligodeoxynucleodtides (ssODN), 2) Cas9 messenger-RNA (mRNA) with small guide (sgRNA) and ssODN, 3) Cas9 mSA with sgRNA and ssODN-biotinylated, and 4) Cas9 mSA with sgRNA and ssODN. Cells were cultured 48 hours after transfection using N2B27 media without antibiotics. Cells were switched to antibiotic media following the first passage after transfection. Experiments were then also performed in C6 (rat glial) cells with the same groups as done in the ES cell lines. This was done to incorporate a restriction site. The experiments were performed in two different cell lines at two different loci in order to compare efficiencies. Results from the ES cells were validated using FACs sorting as the cell line is a GFP which we were converting to BFP, while C6 data was validated using PCR and a restriction digest. The goal of this experiment was to increase fragment KI's and help with small and large insertions.

Lauren E. Rachow – University of Wisconsin - Madison
Michael J. Flister, PhD
Medical College of Wisconsin – Department of Physiology

The Role of TWIST1 in the Breast Cancer Tumor Microenvironment

Background: More than 3.1 million women in the United States have a history of breast cancer, with heritable genetics contributing to approximately 31% of these cases. Cancer-associated fibroblasts (CAFs) are cells in the tumor microenvironment that promote tumor growth, angiogenesis, metastasis, and chemoresistance. TWIST1, a transcription factor, has increased expression in CAFs, suggesting a positive correlation with tumor growth. Little is currently known about TWIST1's effect on other cancer-related genes, so this study's first aim is to discover genetic relationships in TWIST1 upregulated and downregulated CAFs in breast cancer.

Methods: In order to assess the effects of TWIST1 on breast cancer fibroblasts, the CAF1 fibroblast cell line was transduced with TWIST1 lentivirus or GFP lentivirus (control). A second experiment was performed using CAF1 cells that were transfected with TWIST1 siRNA or non-targeting siRNA (control). Total RNA was extracted from each group (n=3-6 per group), followed by cDNA synthesis and the expression of 82 transcripts was analyzed by RT-qPCR.

Results: To determine the relationship between TWIST1 and the 82 targeted genes, the average fold change was determined using qPCR. We found that 62 of these genes' relationships to the TWIST1 upregulated and downregulated samples were significant using a student's t-test. The most significant relationship was between TWIST1 and ANKRD1. The TWIST1 upregulated samples had 0.11 +/- 0.02 ($P<0.01$) fold-decrease of ANKRD1 and the TWIST1 downregulated samples had a 2.02 +/- 0.10 ($P<0.01$) and 1.64 +/- 0.33 fold-increase, respective to the two different siRNAs utilized in the study.

Conclusion: This study shows TWIST1 regulates the expression of other cancer related genes in cancer-associated fibroblasts. The most significant relationship discovered was that ANKRD1 expression is inversely related to TWIST1 expression in breast cancer-associated fibroblasts. These differences in expression lead us to believe that ANKRD1 plays a role in breast cancer progression via deregulation of the development of the extracellular matrix in the tumor microenvironment.

Ciara Jarmain – Milwaukee School of Engineering
Alexander Staruschenko, PhD
MCW Department of Physiology

Characterization of $P2X_7$ Expression Levels in Dahl Salt Sensitive Rats

Background

Hypertension is a worldwide problem that can cause heart disease, stroke, and disability. The kidneys are a significant controller of blood pressure, electrolyte concentrations, and water balance. Recent studies have shown that pharmacological antagonism of the purinergic receptor, $P2X_7$, a ligand-gated non-selective cation channel, may be directly attenuated blood pressure. $P2X_7$ expression also correlates with the electrolyte imbalances and increased infiltration of immune cells which are hallmarks of salt-sensitive hypertension. To further study the role of $P2X_7$ in salt-sensitive hypertension, we created 3 different $P2X_7$ knock-out animals on the Dahl Salt-Sensitive (SS) rat background and assessed the effect of $P2X_7$ genetic ablation on the development of kidney damage and blood pressure. We hypothesized that deletion of $P2X_7$ would attenuate the development of salt-sensitive hypertension when challenged with a high sodium diet.

Method

To test this hypothesis, 3 different $SS^{P2rx7-/-}$ rat lines (m10, m12, m13) were created using CRISPR/Cas9 gene editing. SS^{WT} littermates were used as controls. $P2X_7$ and $P2X_4$ mRNA and protein levels were determined via qRT-PCR and Western blots. For phenotypic analysis, we measured 24hrs blood pressure using radio telemetry. For 3-4 days post telemetry surgery, baseline blood pressures on low salt (0.4% NaCl) diets were determined. Next, the rats were switched to a high salt diet (4% NaCl) for 21 days. Urine was collected weekly, plasma was collected at the termination, and electrolyte levels were analyzed for urine and plasma.

Results

The $P2X_7$ mRNA levels decreased 25% in the m10 line (n=4) and by 45% in the m13 line (n=2), but there was no significant difference due to variability in the m10 line and too few animals in the m13 line. The $P2X_4$ mRNA levels did not change. The Western blot revealed there were no changes in $P2X_7$ or $P2X_4$ protein levels. There were no differences in mean arterial pressure, sodium levels, or potassium levels from the urine and plasma samples. Currently, we are studying the m12 line and their response to the high sodium diet.

Conclusion

The RNA and protein levels did not change between the $SS^{P2X7-/-}$ and wild type rats. This could be due to possible alternative splice variants or insufficient gene editing. We also interrogated the RNA and protein levels of P2X4 and found no differences. We are currently testing the $SS^{P2X7-/-}$ m12 line. These results can help us understand the role P2X7 plays in the kidney on blood pressure regulation.

Reiauna Taylor – University of Wisconsin Madison
Caitlin O'Meara, PhD
MCW Cardiovascular Center

The Effects of Inhibiting STAT3 and STAT6 on Interleukin 13 Signaling

Background: Interleukin 13 (IL13) is an anti-inflammatory cytokine most commonly known for its role in the immune system, specifically B cells and macrophages. In addition to its role in the immune system, IL13 administration has recently been shown to increase cardiomyocyte (CM) cell cycle activity during regenerative wound healing in the heart. IL13 treatment to cultured CMs demonstrated increased ERK and AKT phosphorylation, cell cycle and anti-apoptotic proteins, respectively. The goal of this project was to test the hypothesis that ERK and AKT activation in response to IL13 is mediated through canonical STAT6/STAT3 signaling pathways.

Hypothesis: IL13 mediates the activation of JAK/STAT through the IL13Ra1/IL4Ra heterodimer receptor which leads to increased CM proliferation. We hypothesize that ERK and AKT activaiton is mediated through JAK/STAT signaling. Therefore, we expect that the *in vitro* addition of STAT3 and STAT6 inhibitors in cultured neonatal rat CMs would deactivate JAK/STAT signaling pathways downstream of IL13Ra1/IL4Ra heterodimers. We hypothesize that decreased levels of these phosphorylated, activated proteins (pSTAT6 and pSTAT3) would subsequently decrease pERK and pAKT expression.

Methods: This experiment was carried out through a series of CM isolation protocols from neonatal Sprague Dawley rats at post-natal day 1 or 2 (P1/P2). The isolated neonatal CMs were cultured overnight in 15% FBS DMEM solution at 37℃. CMs were then serum starved for 24 hours before being treated with 10uM of STAT3 inhibitor (n=3) or 100uM of STAT6 inhibitor (n=3) for 30 minutes. Following this, the cells were treated with 20ng/mL of mouse IL13 for 20 minutes and collected. Western blots were then run to measure protein levels of STAT6/pSTAT6, STAT3/pSTAT3, AKT/pAKT and ERK/pERK using GAPDH as a control.

Results: We found that our inhibitors work properly by inhibiting STAT3 and STAT6 transcription factors. Western blot analysis showed that pSTAT3 and pAKT are knocked down in both STAT3 and STAT6 inhibitor treatment groups. However, pERK remained unchanged, indicating that there may be other pathways involved in pERK signaling.

Conclusion: This study showed that inhibiting IL13 signaling through STAT3 and STAT6 decreases downstream signaling proteins pSTAT3 and AKT.

Francesca Mazza – Carroll University
Sang Lee, PhD
MCW Department of Pharmacology and Toxicology

Transmembrane Protein PRR7 Inhibits Secretion of Wnts by Altering GPR177 Trafficking

Background: Synapses are a point of communication between neurons required for signal transmission throughout the brain. Significant synapse loss is correlated with cognitive degeneration in patients with Alzheimer's Disease. Proline rich 7 (PRR7) is a transmembrane protein that promotes synapse elimination by inhibiting Wnt secretion. However, the mechanism behind this is unknown. Wnts are secreted factors responsible for generation and maintenance of synapses. G-protein coupled receptor 177 (GPR177) is a transmembrane protein involved in Wnt secretion. GPR177 is normally localized to the Golgi apparatus where it transports Wnts via secretory vesicles. After transport, GPR177 is recycled back to the Golgi apparatus via endosomal trafficking. We hypothesize that PRR7 inhibits Wnt secretion by blocking normal GPR177 trafficking. This hypothesis was tested using immunocytochemistry and by analyzing the effect of PRR7 on subcellular localization of GPR177.

Method: Cultured COS-7 cells were grown on glass coverslips treated with poly-L-lysine and maintained in Dulbecco's Modified Eagle Medium. Cells were transfected with either HA-PRR7, myc-GPR177, or both. After incubation, cells were fixed using a 4% formaldehyde solution. Cells were permeabilized using a 1x GDB solution and were incubated with primary antibodies, anti-rat-HA and anti-mouse-myc. To determine subcellular localization, GPR177 and PRR7 were either co-transfected with GFP-Lamp1 (late endosome marker), or co-stained with anti-rabbit-Rab5 (early endosome marker), or anti-mouse-Rab9 (late endosome and trans-Golgi marker) antibodies. Cells were then incubated with secondary antibodies conjugated with Alexa488, Cy3, or Alexa 647 for fluorescence. Cells were then mounted onto glass slides. To acquire images, a Nikon C1 plus laser scanning confocal microscope and a 60× objective lens were used. Metamorph and Image J (with Coloc2 plug-in) software were used to measure colocalization.

Results: Results show that in cells transfected with GPR177 alone, Golgi staining of GPR177 was visible. When co-expressed, GPR177 and PRR7 showed a high percentage of colocalization (70-80%) with a Pearson's coefficient of 0.74. Additionally, in cells co-transfected with PRR7, GPR177 had higher colocalization with Rab9- and Lamp1-positive organelles than with Rab5-positive organelles. This suggests that GPR177 is localized to late endosomal compartments in the presence of PRR7.

Conclusion: The high percentage of colocalization between PRR7 and GPR177 suggests that they are trafficked together. In the presence of PRR7, GPR177 is localized to subcellular locations of Lamp1- and Rab9-positive endosomes. This sequestering of GPR177 may inhibit proper Wnt secretion. Further experimenting may determine the pathway and mechanisms that PRR7 uses to localize GPR177 to these specific compartments.

Alexander Morateck - Macalester College, St. Paul MN
Weiguo Cui, MD, PhD
MCW Department of Microbiology & Immunology

Single Gene Modification of Memory T Cells Using CRISPR/Cas9

Background

Immunological memory is the foundation of preventive medicine. Memory T cells are a key component of immunological memory. By designing a guide RNA (gRNA) that matches a portion of a gene of interest, we can utilize a CRISPR/Cas9 system to directly delete those genes and test their function in memory T cell development. We hypothesized that utilizing a pool of gRNAs targeting a set of transcription factors would enable us to better understand the transcriptional networks regulating memory T cell differentiation.

Methods

Forty-five 25bp gRNA oligos were designed to match exons of each gene assessed, with three oligos per target gene. Each pair of oligos was annealed and inserted into a plasmid vector containing a gRNA scaffold, U6-promoters, a fluorescent marker (mCherry), an ampicillin-resistance gene and a unique gene index (UGI). Each ligated plasmid was then transformed into Stbl3 competent cells for amplification and selection. A single colony containing each plasmid was screened initially using colony PCR followed by electrophoresis. Plasmids displaying positive bands on a 1.5% agarose gel were extracted using a Qiagen MiniPrep Kit. Samples were sent for gRNA and UGI sequencing. After obtaining successful sequence results, HEK293 T were transfected to produce retrovirus containing the pertinent gRNA plasmid. UGIs were also compared to make sure gRNA plasmids could be distinguished on the cellular level in the final pool of viral vectors. After high titer viruses were produced, $CD8^+$ T cells expressing Cas9 were activated in vitro, transduced with the gRNA-containing retrovirus, and cultured for 48 hours in the presence of IL-2 (100 unit/ml). FACS was then performed to check transduction efficiency and changes in function and phenotype caused by gene editing. Cells were stored for use in later experiments regarding phenotypic and functional analyses after genes of interest were knocked out.

Results

As hypothesized, transduction and gene modification were successful. Transduced cells were frozen for use in phenotype and function assays in vitro and further function assays in vivo.

Conclusion

Direct modification of memory T cell genomes allows better understanding of memory T cell phenotype and function. Next steps include in vitro assays to assess phenotype and function after gene editing, and in vivo assays to assess response to acute and chronic infection, as well as provide a better understanding of T cell differentiation and proliferation.

Leah Flanagan – Augustana College
Dorothee Weihrauch, Janine Struve, Michelle Bordas, Kennedy Key, Angela Franco, Gabriela Castro
Department of Anesthesiology

Preeclampsia and Signaling Properties within the Placental Extracellular Matrix

Introduction: Preeclampsia (PE) is a disorder developed during pregnancy. It is characterized by increased blood pressure and proteinuria. Complications that accompany preeclampsia include hypertension, fetal growth restriction, preterm birth, organ damage, eclampsia, and is the leading cause of maternal and fetal mortality. The etiology of preeclampsia is uncertain. However, there are findings that suggest preeclampsia may be initiated by abnormal trophoblast invasion of the maternal spiral arteries during placentation. The signaling properties of the extracellular matrix (ECM) in preeclampsia has been an important focus in previous research. Understanding the signaling properties of a preeclamptic ECM could help identify an altered phenotype, leading to further insight of the pathology of preeclampsia.

Objective: We suggest that expression patterns of ECM proteins may contribute to the development of preeclampsia and controlling their expression may serve as a means to regulate placenta function, securing a healthy pregnancy. This instigates our interest in gaining a better understanding of trends in ECM signaling properties in healthy versus preeclamptic placentas.

Methods: Markers investigated included oxidative adducts 4HNE (4-hydroxynonenalis, a lipid peroxidation end product) and AGE (advanced glycation end products), heparan sulfate (role in birthweight and maternal blood pressure control), laminin (important for cell differentiation), galectin-3 (involved in cell-matrix interactions), and collagen-1 (contributes to stiffening blood vessel walls).
Sampling healthy term placentas and placentas affected by late-onset preeclampsia, we fixated frozen sections (10 μm) to slides and treated the sections with various antibodies to visualize ECM components.
Immunohistochemistry was performed. The sections were incubated following primary antibody (1:50) to aforementioned markers and secondary antibody (1:1000) treatment. Goat, anti-goat, rabbit, anti-rabbit, mouse, and anti-mouse blocking agents were utilized. DAPI nuclear stain (1:1000) was used. Fluorescence intensity was determined to identify trends and differences between proteins in normotensive and preeclamptic placenta extracellular matrices.

Results: Following fluorescent intensity analysis, ECM proteins were classified as up- or down-regulated in PE placenta tissue. In our findings, AGE, and collagen were up-regulated, while 4HNE, heparan sulfate, and galectin-3 were down-regulated in PE tissue. Laminin expression was unchanged.

Conclusion: ECM in preeclampsia exhibits an altered phenotype. Heparan sulfate downregulation makes BP regulation more difficult; galectin-3 downregulation influences the cell-matrix interactions like the migration of cells.

Keywords: Preeclampsia, placenta, pregnancy disorder, extracellular matrix

Saurabh Dhole – Texas A&M University
Dr. David Stowe, MD, PhD – Mentor
MCW Department of Anesthesiology Research

Hypothermia Best Protects Cardiomyocytes against Ischemia-Reperfusion Injury by Improving Mitochondrial Bioenergetics and Reducing Mitochondrial Calcium Overload

Background and Hypothesis: Mitochondria (m) are dynamic organelles that are responsible for vital processes such as cellular energy metabolism and initiation of apoptotic cell death following cell stress. Mitochondria consume O_2 (respiration) in the process of electron transport (oxidation). Protons are pumped during electron transport to create the membrane potential ($\Delta\Psi_m$) and proton entry allows ADP to make ATP (phosphorylation). During IR injury, cell calcium accumulates and is buffered by mitochondria so that mitochondrial $_m[Ca^{2+}]$ rises causing a disequilibrium of the ion homeostatic state between cytosolic $_c[Ca^{2+}]$ and $_m[Ca^{2+}]$. $_mCa^{2+}$ overload can cause depolarization of $\Delta\Psi_m$, permeabilization of the inner and outer mitochondrial membranes, and release of cytochrome *c* leading to apoptosis. IR injury occurs when nutrients to the heart are dramatically decreased and the subsequent return of O_2 and nutrients causes damage to tissue. Also electron transport is impeded during IR; this allows generation of the superoxide radical and other reactive O_2 species; moreover, with depolarization of $\Delta\Psi_m$ less influx of protons slows ATP production. These events can initiate mPTP opening to induce apoptotic pathways. Two experimental treatments that reduce IR injury are cardioplegia and hypothermia. It is unclear if cardiac protection by these treatments is associated with improved bioenergetics and reduced $_m[Ca^{2+}]$ loading. Our objective was to investigate if hypothermia treatment better protects cardiomyocyte mitochondria than does cardioplegia treatment by reduced mCa^{2+} loading and improving bioenergetics. To do so, we assessed myocardial function during IR injury and its effect on mitochondrial respiration and calcium retention capacity (CRC). **Methods:** Hearts from rats were isolated and perfused at a constant pressure with Krebs buffer solution (5 mM $[K^+]$). There were four treatment groups: group (time control (TC), no IR at 37ºC, 50 min perfusion; IR (at 37ºC, 20 min baseline, 25 min global ischemia, 5 min reperfusion); IR+CP (cardioplegia) (14 mM$[K^+]$, 37ºC); and IR+HP (hypothermia, 17ºC) applied for 5 min before ischemia and for 20 min on reperfusion). Hearts were minced and centrifuged in isolation buffer to isolate mitochondria. The resulting mitochondrial pellets (12.5 mg/ml) were assessed for Ca^{2+} uptake capacity (CRC) and $\Delta\Psi_m$ by fluorescence spectrophotometry (Fura-4AM and TMRM). CRC = number of $CaCl_2$ pulses (20 mM) until Ca^{2+} uptake was maximal. In addition, respiration was measured by an O_2 electrode in a sealed chamber during state 2 (resting state), state 3 (ATP production), and state 4 (ATP consumed). The respiratory control index (RCI_a) = state 3/state 2 and (RCI_b)= state 3/state 4. Cardiac function was measured by changes in developed left ventricular pressure (systolic-diastolic) = (dLVP). **Results:** We found for TC, IR, IR+HP, and IR+CP groups, dLVP changes (% initial values) at 5 min reperfusion of -2%, -91%, -4%, and -75% respectively. Mean RCI_a and RCI_b in TC, IR, IR+HP, IR+CP groups respectively, were: 8.4, 3.7 (PM), 2.8, 1.6 (Suc); 5.5, 2.3 (PM), 2.6, 1.1 (SUCC); 9.3, 4.1 (pyruvate/malate =PM), 2.0, 1.8 (Succinate substrate=Suc); and 5.2, 4.6 (PM), 2.2, 1.7 (Suc), respectively. The mean CRCs and time to $\Delta\Psi_m$ repolarize for TC, IR, IR+HP, and IR+CP, respectively, were: 8 (PM), 7 (Suc), 69s (PM), 174s (Suc); 7 (PM), 9.5 (Suc), 106s (PM), 300s (Suc); 7.5 (PM), 9.5 (Suc), 57s (PM), 110s (Suc); and 6.5 (PM), 7.5 (Suc), 72s (PM), 133s (Suc). **Conclusions:** Both cardioplegia and hypothermia protect mitochondria isolated after IR injury as assed by RCI and CRC compared to IR alone. However, hypothermia treatment provided much greater cardiac functional protection than cardioplegia; in mitochondria after treatment RCI_a was higher after IR+HP than after IR+CP; CRC was higher after TC and IR+HP than after IR and IR+CP; and time to $\Delta\Psi_m$ repolarization was shorter after IR+HP compared to other groups. We presume that $_m[Ca^{2+}]$ after IR+HP was less than after IR, and perhaps after IR+CP). Cardioplegia and hypothermia both reduce myocardial cell metabolism, the first by arresting cardiac contractility, the second by reducing metabolic rate of cell processes. As in the heart as a whole, hypothermia to 17ºC likely decreases mitochondrial function to 25% of normal (37ºC). We assume that a decrease in the metabolic rate during IR+HP is greater than the decrease in metabolic rate after IR+CP.

Emily Siniscalco – Ithaca College
Michele A. Battle, PhD
MCW Department of Cell Biology, Neuroscience, and Anatomy

The Protective Role of Sensory Neurons and Calcitonin Gene-Related Peptide in Inflammatory Bowel Disease

Inflammatory Bowel Disease, or IBD, is a term encompassing both Crohn's disease and Ulcerative Colitis, which are two diseases involving the inflammation of the gastrointestinal tract. Sufferers of IBD deal with severe pain and discomfort as a result of their condition; however, little is understood about the biological mechanisms influencing IBD. One particularly interesting area of study encompasses the effects of sensory neurons on IBD severity. Current research indicates that sensory neurons play a role in inducing inflammation in the colon; however, new ideas involve a dual role of the sensory neurons: that of both inflammation and protection. In particular, our research focuses on the possible protective role played by sensory neurons through the release of a neuropeptide, CGRP. CGRP is released from sensory neurons expressing TRPA1 ion channels and binds to heterodimer receptors made up of CALCRL and RAMP1 proteins in the cells of the colon epithelium. Since the exact effects of CGRP release are unclear, we aimed to elucidate them through a series of experiments involving the induction of DSS colitis in mouse models, using both wild type mice, as well as mice with a CALCRL conditional knockout (cKO) in the intestinal epithelium. Tissues harvested from these mice were used to determine the level of disease in each animal, as well as various factors indicating the overall effect of the CALCRL cKO including intestinal permeability, weight change, and shifts in cellular niches. Examination of intestinal permeability through a FITC-dextran fluorescence assay revealed a higher level of permeability in CALCRL cKO mice. Additionally, results of q(RT)-PCR indicate a decrease in RNA transcripts marking enteroendocrine and proliferative niches. Combined, these results indicate a higher level of damage in the colons of CALCRL cKO mice as well as a decrease in protective cellular functions. Such results support the protective role of CGRP in colitis and point towards a dual inflammatory and protective role of sensory neurons in the colon during IBD.

Automatic segmentation tumors using a CNN-

DAE <u>Background</u>

The number of papers published on deep learning has exponentially grown each and every year for the past several years. With an increase being seen not only in the medical world, but in medical imaging specifically, as deep learning has shown revolutionary results in reconstruction, artifact removal, and complex computer vision tasks.

Deep learning is used in a variety of tasks: data object identification, computer vision, segmentation, and etc. Deep learning can be this versatile due the structure of the technique making it a universal approximator of functions. This is done through the modulation of data through a series of nodes, weights, and biases (figure 1). These systems are referred to as networks and takes the inputted data through the modulations in a linear fashion, but the weights and biases are randomly initialized and adjusted through a training phase of the network. The training is done through the comparison of a ground truth given a specific dataset being inputted. For example, if the networks task is to identify a handwritten seven as a seven. The input data into the network will be an image of seven, lets say a
28x28 image, and the output will be a single value (1x1), which should be seven. Of course, if the weights are randomly initialized, it will be incorrect to begin with, but with every image that is inputted and ground truth that is compared. The weights and biases are adjusted to approach a network that can accurately accomplish the task at hand: identification of handwritten numbers. After this, the network would be tested on a testing dataset that was not used to train the network, allowing for an understanding on how truly accurate the network is at achieving the task.

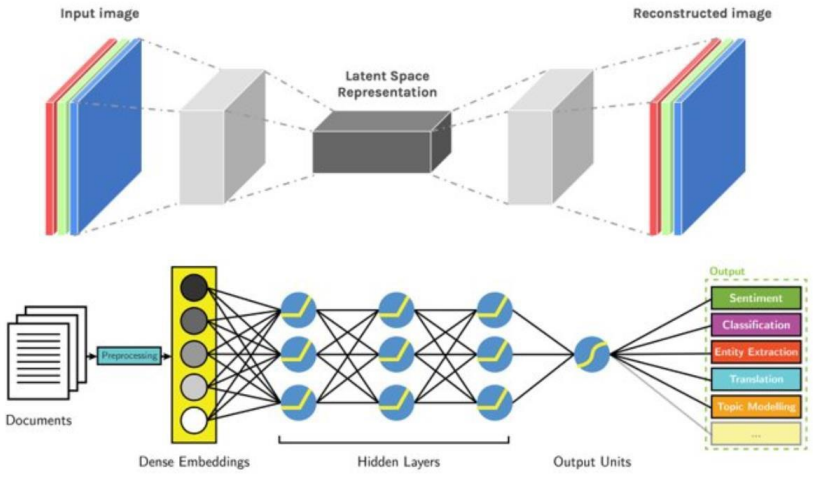

Figure 1: This figure demonstrates the fundamentals of deep learning and how the data is inputted, modulated, and over reduced in dimensionality in a linear fashion to arrive at the wanted output. Bottom figure demonstrates the data being reconstructed on one-dimension, while the top figure demonstrates the premise of convolutional-neural networks and their use in autoencoders, which most matches the architecture used in the study.

The very nature of this training phase makes deep learning able to handle any arbitrary task given enough data to train the network. In our work, this was extended to the tasks of creating a network that would automatically segment high-grade glioblastomas and low-grade glioblastomas. Up until the expansion of deep learning, this task could not be done automatically. As these tumors can appear throughout the brain with various sizes and tissue types, but with the versatility of deep learning. Several other labs have shown promising results; thus a network was developed with inspiration from a multitude of other papers to tackle this task.

Method

BRATS 2015 training and testing data was used to allow for the generation of the network. All subjects in the data had four modalities available: T1, T1-contrast, T2, and FLAIR. In the training, 220 subjects had high-grade glioblastomas and 15 subjects with low-grade glioblastomas (figure 2). In the testing data, 110 subjects were present with a mix of high-grade and low-grade glioblastomas to evaluate the performance.

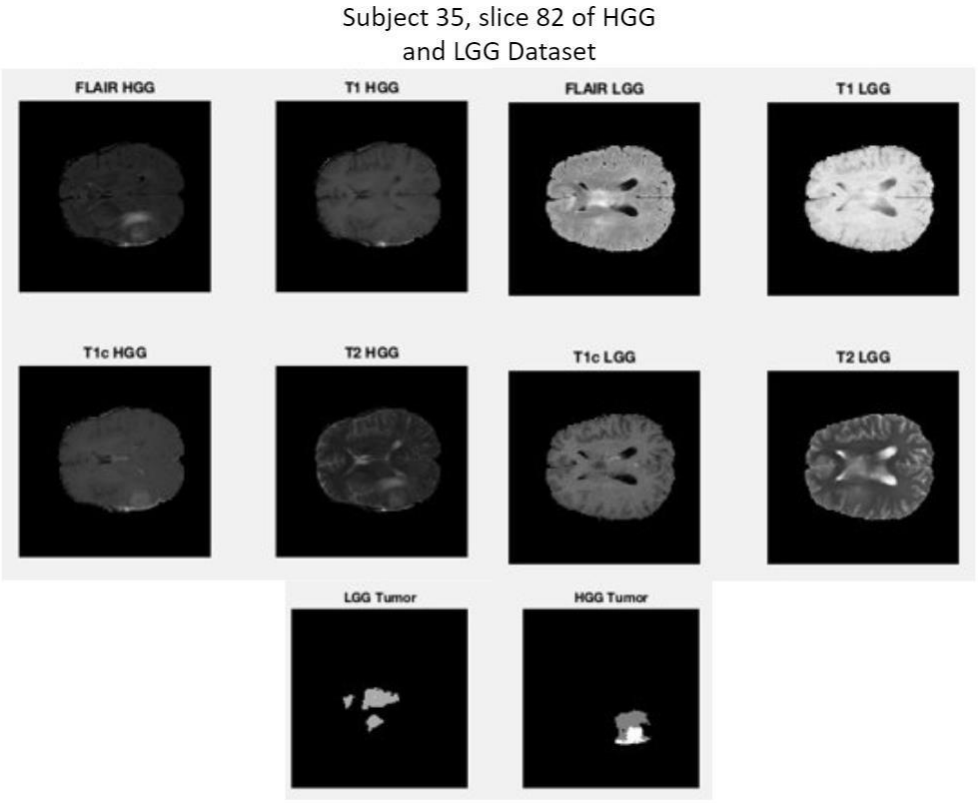

Figure 2: Visualization of the data, demonstrating the input of the data in the four modalities. And the output ground truth that the data is compared against.

A convolutional neural network (CNN) denoising autoencoder (DAE) architecture was chosen. Noted by (Hugo Larochelle, 2017), using multiple pathways with varying kernel sizes can allow the network to not only learn small local features, but more global features. In addition to this, the output of the network is an image as opposed to a label of a pixel. This was done to prevent the issue of independently labeling pixels next to each other, an issue seen in several other papers. Each pathway considered the strengths and weaknesses of each modality, and specific kernel sizes of the CNN were chosen to take advantage of them.

L1 and dropout regularization were both used to prevent overfitting, and Xavier initialization was

utilized in weight initialization to prevent saturation of learning rates with the sigmoid function. In efforts to reduce the number of parameters, optimize the selection of key features, and reduction of overfitting Max-Out networks was applied using a unique script that applied the technique described by (Yoshua Bengio, 2013). This allowed for the most important features to be extracted from the feature maps. Lastly although designing kernels for specific modalities would achieve an understanding of the features in each modality indicative of a tumor, interactions between the modalities can also be helpful in the identification of tumors. And thus an additional pathway was added that performs a local and global analysis of the data with a depth of four, meaning that all modalities are taken into account. After the initial convolutions of all pathways, the results are concatenated, deconvolved and outputted as an image.

All scripts were created and applied through the functional API keras of tensorflow.

Results

The results of this network are tentative, but as the network is heavily inspired by three papers (Ganapathy Krishnmurthi, 2017) (Hugo Larochelle, 2017) (Ruizendaal, 2018). Results are expected to match or exceed them, and their results are demonstrated below.

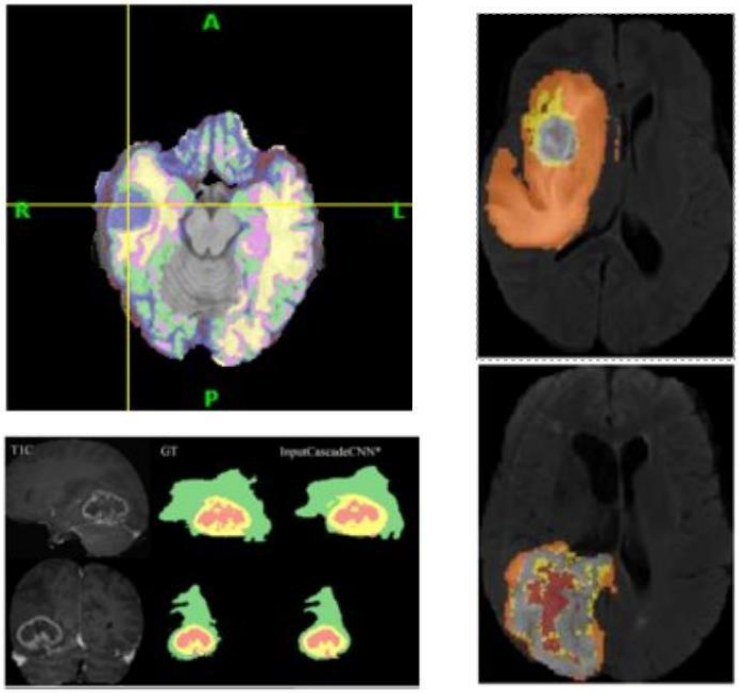

Figure 3: Examples of three different results from architectures similar to the network designed, refer to references for a more in-depth analysis on the architectures corresponding to each result.

Conclusion

In future work, the architectures and hyperparameters will be adjusted to optimize results as well as several preprocessing techniques being implemented (batch normalization, histogram matching, etc.). It is expected that the results will demonstrate that automatic segmentation of brain tumors is

possible and should be preferred. As performing segmentation through these automated techniques would allow for the reduction of the needed time to process tumor scans.

Works Cited

Ayush Jaiswal, V. R. (n.d.). Brain Tumor Segmentation with Deep Learning .

Despois, J. (2017, Feb 7). *Autoencoders - Deep Learning bits #1*. Retrieved from HackerNoon: https://hackernoon.com/autoencoders-deep-learning-bits-1-11731e200694

Ganapathy Krishnmurthi, B. A. (2017). Semi-supervised Learning using Denoising Autoencoders for Brain Lesion Detection and Segmentation .

Hugo Larochelle, M. H. (2017). Brain tumor segmentation with Deep Neural Network. *Medical Image Analysis* , 18-31.

Ruizendaal, R. (2018). *Using Deep Learning for Structured Data with Entry Embeddings* . Retrieved from Towards Data Science: https://towardsdatascience.com/deep-learning-structured-data-8d6a278f3088

Yoshua Bengio, I. J. (2013). Maxout Networks

Jonathan Cobb – Milwaukee School of Engineering
Kathleen M. Schmainda, PhD
Medical College of Wisconsin Department of Radiology

Gallium Maltolate Inhibits the Advancement of Glioblastoma in Rats

Iron is used by cancer cells to promote the production of more aggressive cell populations. Brain tumor cells have been shown to overexpress the transferrin (iron) receptor. We therefore hypothesized that the administration of an iron mimetic, such as Gallium Maltolate (GaM), which targets the transferrin receptor, will inhibit the mitochondrial and enzymatic activity of brain tumor cells, causing cell death. To test this hypothesis, we performed a study to determine if GaM would inhibit the growth of brain tumors in a rat brain tumor model. Human glioblastoma cells were implanted into rat brains, and tumor growth was confirmed using MRI two weeks later. Rats received oral formulations of GaM (50 mg/kg/day) as either daily treatment, or a cycle of on-treatment for two weeks and off-treatment for one week. During this time the tumor growth was monitored using MR imaging, at 9.4 T, once per week. After the rats died, the brains were saved for histological analysis. We found that the GaM treatment was effective. It increased the life span of the treated rats and caused complete tumor regression in 20% of them. Histologically, the tumor cell death appeared similar to tumor cell death resulting from chemotherapy. The histological cell counting analyses revealed significantly fewer active tumor cells in the responding tumors compared to those that did not respond to treatment. A count of the number of mitotic cells per 10 high power fields is a viable way to analyze if the tumor was still active or not. Once completed, this count showed that the treated tumors were much less active, $p = 0.025$. This test showed that, overall, the GaM treatment was mostly effective against glioblastoma in the rats. The test agreed with the original hypothesis, suggesting that this might prove to be an effective treatment against brain tumors in patients. This needs to be tested further, to ensure the results are long-lasting, and that there are no adverse effects that are caused by the treatment.

Emily Ott – Saint Louis University
Rashmi Sood, Ph.D.
MCW Department of Pathology

Role of Platelets in the Placental Pathology of Tissue Factor Pathway Inhibitor deficient mice

Background

Tissue Factor Pathway Inhibitor (TFPI) is a serine protease that regulates multiple steps in blood coagulation. It is alternately spliced with at least two isoforms. The longest isoform, TFPIα consists of an acidic N-terminal region followed by three Kunitz-type domains, and a basic C-terminal region. The first Kunitz domain (K1) is present in all isoforms. It binds Factor VII (FVII) and inhibits blood clotting initiated by Tissue Factor (TF)/FVIIa complex. TFPI serves an important anticoagulant role in embryonic development and survival. When the K1 domain of TFPI is eliminated in mice by genetic targeting, 60% of knockout embryos die in mid-gestation and remaining die at birth. The cause of death of TFPI null embryos and pups is not known, but suspected to involve excessive blood clotting and consumptive coagulopathy. We have shown that a small number of TFPI null embryos survive embryonic development and are born alive if both the mother and father lack the integrin αIIb receptor expressed on platelets. The goal of this study is to examine placental pathology of late stage embryos and to identify a potential role of maternal platelets.

Methods

High resolution Nanozoomer images of TFPI_K1$^{-/-}$ and TFPI_K1$^{+/+}$ placentae from TFPI_K1$^{+/-}$ intercrosses were used to trace and quantify necrotic regions. To determine a role of platelets in the formation of these necrotic regions, pregnancies from αIIb $^{-/-}$ TFPI_K1$^{+/-}$ intercrosses were analyzed 18.5 days post-conception. Embryos and placentae were photographed. DNA was prepared from a small tail portion of the embryos and used for PCR-based genotyping. TFPI_K1$^{-/-}$ and TFPI_K1$^{+/+}$ placentae were formalin fixed, paraffin embedded, sectioned and observed after hematoxylin-Eosin staining for pathology and presence of necrotic regions. To identify the role of maternal versus fetal αIIb, we also analyzed placentae from TFPI_K1$^{+/-}$ male crossed to αIIb $^{-/-}$ TFPI_K1$^{+/-}$ female and the reverse genetic cross.

Results

TFPI_K1$^{-/-}$ placentae had more necrosis than TFPI_K1$^{+/+}$ placentae in pregnancies from TFPI_K1$^{+/-}$ intercrosses (24437±4478 versus 12292±7286 μm^2; P=0.08). Combined absence of αIIb from the mother and the fetus (αIIb $^{-/-}$ TFPI_K1$^{+/-}$ intercrosses) significantly attenuates necrotic areas in both genotypes (355±504 versus 597±2280 μm^2; P=0.7). We are currently analyzing other genetic crosses to identify if maternal or fetal αIIb is responsible for necrotic regions in the placenta.

Conclusion

Our data associates increased placental necrosis with TFPI_K1$^{-/-}$ genotype. We demonstrate that integrin αIIb is responsible for necrotic lesions in both genotypes. The ongoing experiments will allow us to distinguish between roles of maternal versus fetal integrin αIIb in placental necrosis.

George Ronan, Jr. – Marquette University
Dhanush Haspula, Ph.D. – Medical College of Wisconsin
Brain Hoffmann, Ph.D. – Medical College of Wisconsin

Title: The Effects of Artificial Sweeteners on the Concentrations of Plasma Metabolites in Rat

Abstract

Rising rates of diabetes worldwide have drawn attention to many factors that may provide insight into the mechanism of onset of diabetes. Many of these mechanisms are influenced by diet, in particular glucose and other sweet substances. Non-caloric artificial sweeteners have been increasingly added to diets as an alternative to traditional high calorie sugars for reasons such as caloric control and weight management. However, knowledge of the full effect of non-caloric artificial sweeteners on the metabolism is limited and controversial. This study aimed to test the metabolic effects caused by consumption of common non-caloric artificial sweeteners (aspartame and acesulfame potassium) and caloric sweeteners (glucose and fructose). Five groups of rats (n = 6), one control group and four experimental groups, were fed water (control) or sweetener supplemented water for 3 weeks. Blood was then drawn, plasma was isolated, and samples were analyzed via untargeted and targeted high-throughput mass spectrometry-based metabolomics. Results showed that all sweeteners impacted plasma metabolites to varying degrees, with the most extreme alterations being observed as a result of chronic acesulfame potassium and fructose consumption. Metabolites were also characterized according to function and assessed for influence on potentially relevant pathways. Inflammation, oxidative stress, gluconeogenic activity, and other relevant metabolic shifts were observed in these two groups. This study is one of the first of its kind to characterize the changes in the metabolome after consumption of these various sweeteners and will aid in better informing the field of the effects of high dietary consumption of these compounds.

Keywords: Diabetes, Database, Metabolomics, Sweeteners, Metabolism

Title: The Effects of Chronic Exposure to Non-Caloric Artificial Sweeteners on Rat Microvascular Endothelial Cell Function

Authors: Laura Danner[1,2,3,4], Dhanush Haspula[2], Brain Hoffmann[,2,3]

Affiliations: [1]Summer Program for Undergraduate Research, [2]Department of Biomedical Engineering, and [3]Cardiovascular Center, Medical College of Wisconsin; [4]University of Wisconsin – Milwaukee

---

Abstract

As the diabetes epidemic grows worldwide, consumers increasingly consume non-caloric artificial sweeteners (NCAS) as an alternative to caloric sweeteners in beverages and packaged foods. Many Americans consume NCAS daily, but evidence is lacking that chronic consumption of these compounds is safe for overall systemic health, especially those related to the cardiovascular system. This study aimed to test the functional effects of three NCAS (acesulfame potassium, sucralose, and stevia) that get absorbed into the blood on Sprague-Dawley rat cardiac microvascular endothelial cell (RCMVEC) function. Cells were cultured using standard endothelial cell media (control) and media containing varying concentrations of each individual NCAS that mimic an average serving size per fluid ounce. The cells were then tested for functional deviation via tube formation assay at one day, one week, and two weeks of treatment with the sweeteners. Live cell count, cell viability, and reactive oxygen species (ROS) production were measured for each sample at this time. Results varied between artificial sweetener groups, with each sweetener treatment showing significant deviation from control groups. The greatest impact on tube formation was observed with chronic exposure to acesulfame potassium; We also saw acesulfame potassium accumulate at 21 ± 10 μM (N=6) in the blood of rats chronically consuming this compound for three weeks. Sucralose also exhibited altered tube formation, while low concentrations of stevia demonstrated less functional differences on tube formation. ROS production was not significantly impacted in all groups of treated cells. This study is the first to observe the effects of three common NCAS on microvascular endothelial cell function. These studies, along with future analysis, will allow healthcare providers and consumers to make more informed decisions regarding the consumption of these common food additives.

Alexander Zhu – Princeton University
Shi-Jiang Li, PhD
Department of Biophysics

Machine learning classification and denoising in resting-state functional MRI for Alzheimer's disease and cognitively normal patients

Background
Functional magnetic resonance imaging (fMRI) has been useful in detecting the functional connectivity within various regions of the brain and is a significant biomarker for Alzheimer's disease. Of particular use to Alzheimer's disease studies is resting-state functional magnetic resonance imaging (rfMRI), which does not require the patient to perform a cognitive task during the imaging session. Unfortunately, rfMRI contains many sources of noise, reducing the signal-to-noise ratio and complicating statistical analyses. Therefore, removing these noise components is of great importance. One promising but time-consuming method involves independent component analysis (ICA), which separates fMRI data into distinct components, and hand-classification of each component. To catalyze the hand-classification process, studies use FMRIB's ICA-based X-noiseifier (FIX), a machine learning hierarchical classifier that, once trained, can effectively identify and label individual components as noise or signal. FIX is often tasked with denoising rfMRI data from cognitively normal (CN) patients or Alzheimer's disease (AD) patients exclusively, but little has been published on FIX's cross-group success. In this study, we aimed to determine FIX's efficacy of classifying and cleaning rfMRI data from patients with a different stage of Alzheimer's disease from the training set, and subsequently, the similarities of components between AD and CN patients. We hypothesized that these components of AD patients would differ from those of CN patients.

Methods
We preprocessed rfMRI data from 35 AD patients and 48 CN patients using brain extraction, motion correction, and high-pass temporal filtering to remove low-frequency artefacts. We then applied ICA through FMRIB's Multivariate Exploratory Linear Optimized Decomposition into Independent Components (MELODIC). 30 subjects with over five signal components were selected from each group for hand-classification and were divided into 30 combinations of 15 subject subsets. One subset from each group was used to train FIX, while the other was designated as the test set. We then measured FIX's performance with each training set through LOO-style accuracy testing on all 60 test sets. 30 tests from each set were drawn for statistical analysis.

Results
FIX performed well in all four groups: CN vs. CN had a median accuracy of 97.5%, AD vs. CN with 97.0%, AD vs. AD with 97.5%, and CN vs. AD with 97.1%. Wilcoxson rank sum tests on every combination of groups revealed no statistically significant difference between medians at a threshold of 20, with all p-values above 0.05.

Discussion
With no statistically significant difference between any group's medians, we conclude that the signal and noise components of AD patients and CN patients are more similar than previously expected. This eliminates the need to hand-classify separate training sets for studies involving both conditions, saving time and effort.

Jessica C. Jurak – Southern Illinois University, Carbondale
Michael Lerch, PhD
MCW Department of Biophysics

Effects of Palmitoylation on the β_2-Adrenergic Receptor

Background

G protein-coupled receptors (GPCRs) are responsible for regulating nearly every physiological process of the human body, which makes them great candidates for drug development. GPCRs rely on a high degree of conformational flexibility to achieve their signaling complexity, and one of the major goals of structure-based drug design is to identify conformations associated with a particular signaling profile. Post-translational modifications, such as palmitoylation, modulate receptor activity, yet their effect on receptor structure and dynamics remains largely unknown.

Method

In this study we will monitor the impact of palmitoylation on the local structure and dynamics within the β_2-adrenergic receptor (β_2AR) using site-directed spin-labeling (SDSL) in combination with electron paramagnetic resonance (EPR). This involves site-specific introduction of cysteine residues, which are subsequently reacted with a thiol-specific reagent containing a stable unpaired electron in the form of a nitroxide (a "spin label"). We plan to measure the effect of palmitoylation on the local dynamics by placing spin labels nearby the palmitoylation site, and to measure allosteric effects using spin labels in regions that undergo critical conformational changes upon activation of the receptor.

Results

For this project, I introduced cysteine mutations within a minimal-cysteine β_2AR construct through site-directed mutagenesis. I engineered a total of twenty-four constructs, with cysteines placed at twelve sites in each of two variants of the β_2AR, one with the native palmitoylation site intact and one with it removed. These twelve sites were chosen based on their location near the palmitoylation site in helix 8. Certain sites, such as S345 and S346, for example, were chosen because they are phosphorylation sites known to be influenced by palmitoylation. Additionally, I optimized thiol assay conditions for quantifying spin-labeling efficiency and palmitoylation levels, using T4 lysozyme as a model protein in place of the β_2-adrenergic receptor. Preliminary data suggests that the assay is minimally influenced by the salt concentration and pH level of the reaction buffers.

Conclusion

The next steps of this project include identification of viable constructs for EPR experiments from the library I created. The new receptor constructs will be expressed, purified, and subjected to functional assays. The thiol assays will be used to evaluate the palmitoylation level of the receptor and the efficiency of spin-labeling.

Morgan Ford

Peter LaViolette, PhD, MS

MCW Department of Biomedical Engineering

Algorithmically Segmented Pathomic Features of Prostatic Slides for Analysis

BACKGROUND: One in seven men will be diagnosed with prostate cancer in their lifetime. A positive biopsy is typically followed by surgery, when the final diagnosis is done by a pathologist reading tissue samples. Urological pathologists use the Gleason score (G) for classifying prostate tumors, where a G4+ is considered high-grade. The Gleason classification is based on the morphology of individual glands, where each grade of cancer deforms the prostatic glands differently. Therefore, glands with different types of cancer can be categorized by different morphological metrics. The goal of this project was to create an algorithm for morphologically segmenting individual glands to extract histo-morphometric characteristics to determine quantitatively what features drove classification into different grades.

METHODS: Ten whole mount histology slides were digitally scanned from two patients following prostatectomy for known prostate cancer. Custom code was developed in Matlab for identifying morphometric characteristics of individual glands. The morphological segmentation began with color thresholding of the stained slides. The purple cells were then labeled as epithelium, with the white space within each gland epithelium labeled as lumen. The segmentation was tested on a small portion of the slide for accuracy, then applied to the whole slide. Once the segmentation process was complete, the segmented glands were separated by grade using overlaid pathologist's annotations. The obtained histo-morphometrics of solidity, wall thickness, and Euler number for each grade classification averaged and compared statistically.

RESULTS: The solidity of benign glands was found to be significantly different from cancerous glands, with P value less than 0.001 (Student's t test), while thickness and Euler number were not found to be significantly different comparing cancer to not cancer.

DISCUSSION: The methods outlined in this study can be used to separate different glands into cancer and noncancerous tissue. Future studies on larger datasets may be used to train automatic classification algorithms to aid pathologists.

James Davis – Milwaukee School of Engineering
Peter LaViolette, PhD
MCW Department of Radiology and Biomedical Engineering

Development of a Graphical User Interface for Quickly Classifying Brain Cancer Histomorphometrics

Background: Glioblastoma is the most common form of primary brain cancer and is highly lethal. Following surgery, pathologists typically diagnose histological samples using a microscope. A similar approach is used at autopsy, where much larger tissue samples are available. Diagnostic features of the samples are recorded for each sample and reported in text, which is uploaded to the medical record in a PDF autopsy report. This process, however, provides an extremely limited dataset of histo-morphometric characteristics for big data analytics and limits the ability for researchers to train and create algorithms to assist in the detection of brain tumors. The goal of this project was to create a graphical user interface (GUI), that would make for easier to record histo-morphometric characteristics detected by pathologists.

Methods: Approximately 2200 photos taken of histology at 10X and 40X magnification were sorted from a large dataset of digital histology acquired from three patients undergoing an autopsy, later diagnosed with two patients having Glioblastoma and one having Adenocarcinoma brain tumors. Custom code was developed in Matlab to create two GUIs (10X and 40X magnification) used to show a pathologist a histology photo from one of the three patients, and a list of checkboxes for a pathologist to use as characteristics to decide whether a picture contained a tumor or no tumor. As the pathologist(s) checked off the characteristics for each picture, they would press next to access a new picture and repeat the process over. To access the results, every time the pathologist pressed next, the Matlab code sent their results in a table as new .mat file, which we were able to open. With enough results, we could generate a deep learning algorithm that can detect a tumor versus and non-tumor by looking at these characteristics.

Results: We were only able to produce the results for two untrained readers. The two untrained readers assigned to detect cancer agreed only about 59 percent of the time on whether a picture contained a tumor or non-tumor. There was not enough time to have trained pathologists complete the task, which is ongoing.

Conclusion: The GUIs provide pathologists with a simple to use interface for labeling photos of histology with histo-morphometric features of interest. More data is currently being collected for research purposes. The results we achieved in the proof of concept study with untrained readers demonstrates the importance of having multiple readers interpret overlapping photos. It will also be important to study the test-retest reliability of each individual pathologist.

Grace Callan – Marquette University
John D. Imig, PhD
MCW Department of Pharmacology and Toxicology

DUAL ACTING SOLUBLE EPOXIDE HYDROLASE INHIBITOR/FXR AGONIST, DM509, REDUCES LIVER FIBROSIS IN NONALCOHOLIC STEATOHEPATITIS (NASH)

Background: Nonalcoholic steatohepatitis (NASH) is a global health concern projected to be the leading cause for liver transplantation in developed countries by 2020. NASH can develop from nonalcoholic fatty liver disease and is characterized by lipid accumulation and fibrosis in the liver. If untreated, NASH may progress to liver cancer or cirrhosis. In this project, we explore the dual acting molecule DM509 as a possible treatment for NASH. One of the two functions of DM509 is the inhibition of the enzyme soluble epoxide hydrolase (sEH) which metabolizes epoxyeicosatrienoic acids (EETs) necessary to protect the liver and mitigate hepatic fibrosis. Additionally, DM509 activates the transcription factor farnesoid x receptor (FXR), which in turn activates genes that decrease steatosis and regulate lipid and glucose metabolism. We tested the hypothesis that DM509 will reduce hepatic steatosis and fibrosis by administering DM509 orally to mice with diet-induced NASH. **Method:** Mice were divided into three groups (n=6/group). Group 1: Diseased model group in which methionine-choline deficient (MCD) diet+vehicle results in NASH phenotype. Group 2: Treatment group given MCD diet+DM509 (10mg/kg/d). Group 3: Control group given methionine-choline sufficient (MCS) diet+vehicle. At the termination of the 28-day study, liver tissue was collected for histology and immunohistology. Using histological staining, the liver was assessed for lipid accumulation (Oil Red Staining) and the fibrotic markers collagen (Picrosirius Red Staining) and α-smooth muscle actin (α-SMA, immunohistology). The fraction of area positive for lipid, collagen, and α-SMA relative to total area was calculated using the Nikon Eclipse 55i microscope under 20x magnification and analyzed using the NIS imaging software. **Results and Conclusion:** We found that DM509 has no effect on steatosis; however, it attenuates the fibrotic indicators collagen by 13% and α-SMA by 42%, decreasing fibrosis in the liver. Thus, DM509 reduces hepatic collagen and α-SMA, demonstrating DM509 is an effective anti-fibrotic molecule that could be used as a potential treatment for NASH.

Brian Li – Washington University in St. Louis
John D. Imig, PhD
MCW Department of Pharmacology and Toxicology

Effect of the dual-acting molecule PTUPB in treating kidney injury caused by the anti-cancer drug sorafenib

Background: Sorafenib is an anti-cancer drug that acts as an inhibitor of vascular endothelial growth factor (VEGF), which in turn hinders the process of angiogenesis. Although sorafenib is an effective chemotherapy agent, VEGF inhibitors cause hypertension, kidney damage, and other cardiovascular side effects that often prove to be fatal. PTUPB is a novel drug that acts as a dual acting cyclooxygenase (COX-2) and soluble epoxide hydrolase (sEH) inhibitor, and has the potential to treat kidney injury in multiple pathologies. **Aims/Objective:** This study aimed to test the effectiveness of PTUPB in treating sorafenib-induced kidney injury in rats. **Methods:** Sprague Dawley rats (8-12 weeks old) were given an 8% high-salt diet and were administered either vehicle or vehicle and sorafenib (20 mg/kg/day) for 56 days. The control group (n=4) received only vehicle, and the sorafenib group (n=4) received sorafenib daily through pudding. The sorafenib and PTUPB group (n=4) received sorafenib daily through pudding throughout the protocol, but was also surgically administered PTUPB using an osmotic pump after 28 days of sorafenib treatment. Body weight was measured on days 0, 28, and 56, while blood pressure (tail-cuff method) was measured weekly. At the end of the 56-day protocol, kidney tissue and urine were collected. Biochemical analysis was done on each rat to determine the urinary excretion of protein, albumin, and monocyte chemoattractant protein-1 (MCP-1). Additionally, histological analysis was performed on the cortex of the kidneys to determine renal fibrosis (via Picrosirius red staining) and tubular cast formation (via Periodic Acid Schiff Staining). **Results:** By day 28, sorafenib-treated rats had become hypertensive when compared to the control. The sorafenib-treated rats also had elevated urinary excretion of protein, albumin, and MCP-1 compared to the control by the end of the protocol. After PTUPB was administered, the high blood pressure was attenuated, and urinary excretion of protein, albumin, and MCP-1 were reduced. Also, the sorafenib-treated rats exhibited significant renal fibrosis and renal tubular casts compared to the control group. PTUPB was shown to treat the histological damage of the kidneys in sorafenib-treated rats. **Conclusion:** These results show that the novel dual-acting inhibitor PTUPB has the potential to treat sorafenib-induced hypertension and kidney injury.

Bianca Ruffolo – University of Wisconsin - Parkside
Jeffrey Medin, PhD, MACC Fund Professor
MCW Departments of Pediatrics and Biochemistry

Chimeric Antigen Receptor Design for Multiple Myeloma and Lymphoma

Introduction

The goal of this study is the development of novel chimeric antigen receptors (CARs) for the treatment of multiple myeloma (MM) and lymphoma. CARs can be transduced into T-cells for targeted attack of cancer cells. Often CARs will encode a single chain variable fragment (scFv) derived from an antibody, which binds to an extracellular target expressed exclusively on tumor cells. The Medin lab has many targets and antibodies in various stages of development. The first part of this study focused on expressing and purifying the extracellular domain (ECD) of a target for MM. The second part focused on mapping the epitopes recognized by antibodies for a lymphoma target.

Methods

A plasmid encoding the ECD of the MM target with a His6 affinity tag was transformed into *E. coli*. The identity of the plasmid was verified by sequencing and test digests. The protein was then expressed in an Expi293 tissue culture expression system and purified using a nickel resin. SDS-PAGE and Western blot with antiHis6 antibody and an antibody specific to the target confirmed expression of the protein and purification via its His6 tag.

The lymphoma target epitope was determined by panning the antibody against a 12-mer phage display peptide library. Peptides that bound to the antibody were detected by immunoblot and their DNA was isolated and sequenced. The sequence was compared with the lymphoma target protein's ECD.

Results

The identity of the MM target plasmid was confirmed. When transfected into the Expi293 expression system, a Western blot confirmed protein product secreted into the supernatant as well as retained in the cell. Western Blot and coomassie staining indicated that the protein secreted into the supernatant was purified via the His6 affinity tag.

The lymphoma target epitope was found to be YFDPTFEWPLM. This sequence has no significant similarity to the ECD of the lymphoma target or to the epitope of a commercially available antibody (determined by the Medin lab) indicating that the epitope is likely conformational. In contrast, the commercial antibody has three regions of sequence alignment with the ECD of the lymphoma target.

Conclusion

Further work will be done to optimize the His6 protein purification. Once it is purified in sufficient quantity, the protein will be used to pan an scFv phage display library in order to identify antibodies for future CAR development.

The anti-lymphoma antibody developed in the Medin lab is distinct from the commercial antibody. The next step in the project will utilize an ELISA to further confirm the identity of the purified lymphoma target.

Mallorie Larsen – University of Wisconsin-Green Bay
John F. Langenheim, PhD
MCW Department of Pathology

EXAMINING THE LACTOGENIC AND SOMATOGENIC ACTIVITIES OF HUMAN GROWTH HORMONE AND HUMAN GROWTH HORMONE VARIANTS ON BREAST CANCER CELLS

Background Growth hormone (GH) and prolactin (PRL), through their receptors, play a central role in mammary ductal and alveolar development and differentiation. The GH receptor (GHR) and the PRL receptor (PRLR) are structurally similar and share common signaling pathways. GH has growth-promoting and metabolic effects in various tissues and PRL is essential for regulation of lactation in rodents. Multiple studies have demonstrated that cancerous human breast tissues express GHR and PRLR, and that both GH and PRL can influence development and/or behavior of breast cancer cells. Human GH is unusual compared to other species in its ability to bind to both GHR and PRLR. Since human GH can activate both GHR and PRLR, it is not clear how each receptor system contributes to the effects of human GH on breast cancer. To address this issue, we produced two recombinant human GH variants reported to have high affinity for GHRs but low affinity for PRLRs. The effects of each hormone on signal transduction, cell proliferation and putative cancer stem cell markers (CD44/CD24) were examined in a breast cancer cell line.

Method GH variants were produced by standard recombinant techniques and expressed using an *E. coli* host-vector system. The recombinant proteins were expressed intracellularly and separated from host cell components using detergents and mild denaturants and the insoluble fraction containing the recombinant proteins was recovered by centrifugation. The recombinant proteins were denatured and reduced, and the proteins were refolded and purified simultaneously using gradient size-exclusion chromatography. The GH variants were dialyzed in a carrier buffer, concentrated by ultrafiltration and filtered sterilized. Homogeneity was confirmed by SDS-PAGE under non-reducing and reducing conditions using Coomassie blue stain. The ability of GH, PRL and the two GH variants to (1) bind to GHRs and PRLRs and activate signaling pathways, (2) mediate breast cancer cell proliferation and (3) induce cell differentiation were examined.

Results Using IM-9 lymphoma cells which only express GHR, the GH variants were confirmed to have a high affinity for GHRs. In T-47D breast cancer cells, which were found to express GHR and PRLR, the activation of signaling was reduced in response to the GH variants relative to that of GH. Likewise, cell proliferation and differentiation were reduced in response to the GH variants relative to that of GH.

Conclusion These findings indicate that most of the biological effects of GH are mediated via the PRLR in the T-47D breast cancer cell line.

Rachel Mutchler – University of Wisconsin Parkside

Jeffrey Medin, PhD, MACC Fund Professor

MCW Departments of Pediatrics and Biochemistry

Antibody Characterization and Protein Purification for CAR T-cell Therapy

Background

The emerging technology of Chimeric Antigen Receptors (CARs) is a new field of personalized cancer treatment which 'arms' a patient's own T cells with a synthetic receptor that specifically targets cancer cells. One way to engineer a CAR is to produce antibodies against the purified extracellular domain (ECD) of proteins that are known cancer antigens, characterize these antibodies, and redesign them into single chain variable fragments (scFvs) to produce the antigen binding domain of the CAR. This project focused on the characterization of antibodies which target Hodgkin and T-cell lymphomas, and the purification of the ECD of a protein expressed in acute myeloid leukemia (AML).

Methods

To identify the epitope of 2 anti-lymphoma antibodies a 12-mer phage display peptide library was bio-panned 3 times to enrich for peptides that specifically bind to the antibody. A dot blot was performed on phage plaques to identify specific clones, twelve plaques were selected, and the phage DNA sequenced.

To express and purify the ECD of an AML-associated protein, a plasmid encoding the ECD with a His6 tag was transfected into Expi293 cells. The transfected cells were grown for 5 days, until viability decreased below 60%. Cell pellets and supernatants were collected beginning on day 3. SDS-PAGE, coomassie-staining, and Western blots with anti-His6 and anti-Protein antibodies were performed to determine the day of optimal protein expression. The protein was purified using a nickel column to isolate His6 tagged protein.

Results

Sequencing results for neither Antibody 1 nor Antibody 2 revealed a consensus for epitope binding.

The ECD of the AML protein was expressed by the transfected cells in increasing amounts over a course of 5 days. The expected protein size was 22 kDa, however, the size detected was around 37 kDa. The column purified AML-associated protein contains bands of higher molecular weight contaminants and not all the protein was eluted from the resin.

Conclusion

The lack of a consensus sequence suggests that neither Antibody 1 nor Antibody 2 bind linear epitopes. In future experiments, other methods, such as site-directed mapping, may be required in order to map the conformational epitope for these antibodies.

Conditions need to be optimized for protein purification, after which a large scale Expi293 culture will be grown to purify sufficient protein for antibody development.

After antibody production and characterization, the CAR sequences will be designed and packaged into lentivirus. *In vitro* testing will be done, and the CARs will then be assessed *in vivo* using AML and lymphoma mouse models.

Sara B. Rubovits—Mount Mary University
Cecilia J. Hillard, Ph.D.
MCW Department of Pharmacology and Toxicology

Does the Endocannabinoid System Play a Role in the Analgesic Effects of Gabapentin?

Background
The endocannabinoid system has long been known to participate in pain modulation, making understanding its mechanisms important in the development of relevant therapeutics. In this study we examined the effects of WIN 55212-2 (WIN), an endocannabinoid receptor (CBR) agonist, and gabapentin, an anti-seizure and neuropathic pain medication. Previous research has indicated a correlation between the use of the gabapentin and levels of circulating endocannabinoid molecules in hospital patients. Previous research also indicates that gabapentin does reduce pain even in CB1R knockout mice, indicating CBR are not required for (but may facilitate) its action. Furthermore, previous studies showed that CB1R knock out mice exhibited an exaggerated response to pain which was reduced by gabapentin treatment. These data suggest that gabapentin and CB1 receptor endogenous activity are mechanistically linked. We examined the interactions between WIN and gabapentin in the context of an inflammatory pain response to determine if the endocannabinoid system contributed to the analgesic effects of gabapentin.

Method
Four treatment groups of n=8 mice were used. One group received gabapentin and vehicle, one received WIN and vehicle, one received both gabapentin and WIN, and one group received only the vehicles. Gabapentin was administered at a dose of 30 mg/kg and WIN at 0.2 mg/kg. The drugs were injected intraperitoneally followed by a hind paw injection of 20ul of a formalin solution (0.925% formaldehyde in PBS) after 15 minutes. 60 minutes of behavioral data from each mouse was analyzed for indications of pain using the Any-Maze software program by recording the amount of time the mice spent attending to the injured paw.

Results
Control animals exhibited the highest levels of pain and irritation in response to the formalin injection. When compared to the control, pain behaviors were significantly decreased by the administration of gabapentin ($p=0.0002$) and WIN ($p=0.0323$) individually. However, two-way ANOVA indicates that there is no interaction between the effects of the two drugs ($p=0.3280$). Thus, the effectiveness of each drug was not influenced by the presence of the other.

Conclusion
Based on our results, it is possible that gabapentin and WIN may be having an additive rather than a synergistic effect. They are potentially utilizing the same pathway, explaining the minimal additional analgesic effect of combining the two drugs. We believe gabapentin may be working downstream of the CBR mechanism, potentially utilizing the NMDA complex to prevent glutamate release or action in the pain circuit. These effects may be enhanced by, but do not require, CBR activation. Additional exploration of this conclusion is needed. Further directions of this research could include manipulating the dose of gabapentin to evaluate the relationship between the two drugs further. There is some concern about gabapentin having potentially addictive properties, so examining its efficacy at lower doses when combined with other drugs may have therapeutic significance.

Kahaan Patel – University of Wisconsin - Madison
Ramani Ramchandran, PhD
Department of Pediatrics

Vasculogenesis and angiogenesis have become an integral part of today's developing field of cardiovascular care, especially in a population where aging and physiological deformities have resulted in vascular abnormalities. Angiogenesis refers to the process by which new capillaries emerge from pre-existing structures, whereas vasculogenesis is the formation of new blood vessels from angioblast precursor cells. Based on preliminary studies done using MVECs (Mouse Endothelial Cells), we tested the hypothesis that PKD1 signaling promotes arteriolar differentiation of microvasculature in vivo. PKD1 can be upregulated using different stimuli. The compounds we tested are Lysophosphatidic acid (LPA) and GS4012, an inducer of Vascular Endothelial Growth Factor (VEGF), both of which have been shown to promote PKD1 signaling. The Zebrafish model was used for this project because of their rapid embryonic development, transparency of embryos, and ability to produce large amounts of embryos. Transgenic Zebrafish embryos Tg(flk1:gfp) were incubated in water containing 20 μM LPA or 3.2 μg/mL of GS4012 at 6 hours post fertilization, and effects upon arteriogenesis were analyzed using in vivo fluorescence imaging. This showed that LPA led to a significant increase in the number of Intersomitic Vessels (ISVs) and inhibited the development of dorsal longitudinal anastomotic vessels (DLAV), whereas GS4012 inhibited caudal vein plexus development. In order to verify if the effects of the compounds were due to the upregulation of arterial proteins, we analyzed the embryo lysates using a Western Blot protocol. Embryos incubated in LPA and GS4012 had EphrinB2 protein expression levels that were, respectively, 2.75 and 1.05 times as much as that found in control embryos. In conclusion, it was found that LPA greatly increases the production of arteriogenic protein markers such as EphrinB2, while GS4012 tends to have a milder effect. This information will be used to further studies on these compounds and develop a method by which vasculature rescue may occur in the future.

Steven Traeger – Lawrence University
Lisa Fraser, PhD
Nita Salzman, MD, PhD
MCW Department of Pediatrics and
Department of Microbiology and Immunology

Production and Stability of Enterococcus faecalis-derived membrane vesicles

Extracellular vesicles (EVs) are nano-sized membrane bound structures released by all domains of life. EVs produced by Gram-positive bacteria are specifically called membrane vesicles (MVs). MVs contain bioactive molecules such as proteins, nucleic acids, nutrients, virulence factors, and toxins. Through the transport of their contents to other bacteria or host cells, MVs serve as an important mode of bacterial communication. MVs are therefore able to play a role in pathological processes, including immune evasion and biofilm formation.

We are interested in studying the role of MVs in the interaction between the Gram-positive pathobiont, *Enterococcus faecalis* (EF), the intestinal commensal microbiota, and the mammalian host GI tract. Our lab demonstrated that EF releases heterogeneous MVs in a strain-dependent manner. To allow us to use EF-derived MVs for future experiments, we sought to determine their stability under a variety of conditions, using two common EF strains, OG1 and the vancomycin-resistant strain, V583.

To determine the stability of EF-derived MVs we used both nanoparticle tracking analysis (NTA) to measure particle concentration and transmission electron microscopy (TEM) to confirm the presence of MVs. We isolated MVs, aliquoted and stored them at -80, -20, 4, 22, and 37^{o} C. We evaluated particle concentration at each temperature, at time 0 and after storage for 1 or 7 days. We verified the presence of MVs in each sample using TEM.

We found that storage negatively impacted particle concentration, with the greatest loss in the first 24 hours. Greater losses of MV particle concentration are seen at higher temperatures. Confirmation of MV presence by TEM is pending.

Although we have determined the stability of intact MVs, we have not yet evaluated their cargo or its stability. Nor have we characterized their heterogeneity. Future directions will include evaluation of stability over an extended time course, as well as the characterization of EF-derived MV cargo and its dependence on strain and growth conditions. We will then use these tools to investigate the role of EF-derived MVs in EF-microbiome and EF-host interaction in the GI tract.